

Form Approved  
OMB No. 0704-0188

[illegible]

19960719 017

OFFICE OF NAVAL RESEARCH

Grant or Contract N00014-93-1-0904

R&T Code 3134037ess08

Scientific Officer: Dr. John Pazik

Technical Report No. 30

"Substitution in  $\text{Ce}_2\text{TSi}_3$  Intermetallic Compositions with  
 $\text{T} = (\text{Cr, Mn, Fe, Co, or Ni})_x(\text{Pd or Au})_{1-x}$ "

by

R.A. Gordon, C.J. Warren, M.G. Alexander, F.J. DiSalvo  
and R. Pottgen

Submitted to

Journal of Alloys and Compounds

Cornell University  
Department of Chemistry  
Ithaca, NY 14853

July 10, 1996

Reproduction in whole or in part is permitted for any purpose  
of the United States Government

This document has been approved for public release  
and sale; its distribution is unlimited

# Substitution in $\text{Ce}_2\text{TSi}_3$ Intermetallic Compositions with $\text{T} = (\text{Cr, Mn, Fe, Co, or Ni})_x(\text{Pd or Au})_{1-x}$

R.A. Gordon, C.J. Warren, M.G. Alexander<sup>1</sup> and F.J. DiSalvo<sup>2</sup>  
*Department of Chemistry, Cornell University,  
Ithaca, NY, USA 14853-1301*

R. Pöttgen<sup>3</sup>  
*Max-Planck Institut für Festkörperforschung  
Heisenbergstrasse 1,  
D-70569 Stuttgart, Germany*

To be submitted to the Journal of Alloys and Compounds

---

## Abstract

Alloys of composition  $\text{Ce}_2(3d/\text{T})\text{Si}_3$ , with "3d" one of Cr, Mn, Fe, Co or Ni and "T" being Pd or Au, were prepared and examined by powder x-ray diffraction. Select single phase compositions were further examined by magnetic susceptibility, by resistivity for the Pd and Co end-members and by specific heat for  $\text{Ce}_2\text{CoSi}_3$ . For compounds not containing cobalt, effective cerium moments consistent with trivalent cerium were observed. A re-examination of the  $\text{AlB}_2$  related structure of  $\text{Ce}_2\text{CoSi}_3$  by single crystal methods revealed ordering of cobalt within the  $\text{CoSi}_3$  hexagonal layer. Magnetic susceptibility, resistance and specific heat measurements suggest valence fluctuation behavior of the cerium in  $\text{Ce}_2\text{CoSi}_3$ . A return to trivalent cerium magnetic behavior occurs on increasing palladium or gold substitution for cobalt.

---

Keywords: cerium intermetallic, valence fluctuation, magnetic susceptibility

---

<sup>1</sup> present address: Dept. of Physics, Seton Hall University, South Orange, NJ 07079

<sup>2</sup> corresponding author

<sup>3</sup> present address: Anorg.-Chem. Institut, Universität Münster, 48149 Münster, Germany

## Introduction

Certain structure types allow considerable substitution of isoelectronic or aleovalent elements without a change in structure. Perhaps the most well-known structure type which exhibits this flexibility is that of  $\text{ThCr}_2\text{Si}_2$ . Cerium-based silicide versions of this composition are known for transition elements Mn through Cu, Ru through Ag and Os through Au [1, 2]. Germanium, arsenic and phosphorous variants in place of Si are also known for some of these transition elements [1, 2].

The ability to substitute extensively in a cerium intermetallic allows some measure of control over electron count and over the variety of atoms in the co-ordination environment of the cerium. If the substitution is by the alloying of elements, some randomness in the type of near-neighbours may be present, unless the alloyed elements order, but the co-ordination number and geometry do not change dramatically. The ability to adjust electron count may allow the Fermi level in such a material to be moved closer in energy to the cerium  $4f^1$  energy level. Alloying may also change the character and overlap of the states near the Fermi level. Both may encourage the formation of a fluctuating or intermediate valence state of the cerium. It is with this in mind that we examine the effects of alloying transition metals (T) in " $\text{Ce}_2\text{TSi}_3$ " compositions.

Numerous ternary rare earth and actinide compounds have been reported with atomic ratios of 2:1:3 [3-8] and adopt variants of either the tetragonal  $\alpha$ - $\text{ThSi}_2$  or hexagonal  $\beta$ - $\text{ThSi}_2$  ( $\text{AlB}_2$ ) structure types [1] (Fig. 1). Several ordered variants of the  $\text{AlB}_2$  structure type are also known:  $\text{Er}_2\text{RhSi}_3$  ( $2a$ ,  $2c$ )[3, 5],  $\text{Lu}_2\text{CoGa}_3$  ( $2a$ ,  $2c$ )[5] and  $\text{U}_2\text{RuSi}_3$  ( $2a$ ,  $c$ )[8]. The type of hexagonal ordering is given in parenthesis and refers to how the ordering has resulted in multiplication of the lattice constants of the  $\text{AlB}_2$  structure type. Cerium-transition element-silicides with a 2:1:3 stoichiometry are reported for T = Co [10], Ni [11], Cu [12] and Rh [3]. An iron version was reported [13] but was not detected in later attempts [14, 15]. The series

$\text{Ln}_2\text{PdSi}_3$  is known for  $\text{Ln} = (\text{Pr}, \text{Nd}, \text{Gd}, \text{Tb}, \text{Dy}, \text{Ho}, \text{Er}, \text{Tm} \text{ and } \text{Y})$  [4], adopting the  $\text{Er}_2\text{RhSi}_3$  structure type, but a cerium member of the series was not reported. Our current study has focused on substitution between the mid to late 3d elements and palladium or gold in  $\text{Ce}_2(3\text{d}/\text{M})\text{Si}_3$ . These larger 4d and 5d elements are chemically very distinct from the 3d elements (apart from some Ni/Pd familial relationship) and may illustrate structural tolerance in terms of different bonding characteristics as well as electron count more so than 3d/3d alloying.

## Experimental

Samples were prepared by arc-melting elements of at least 99.9% purity in the desired atomic ratio. Samples to be annealed were placed in sections of tantalum tubing, then sealed in evacuated quartz tubes. Annealing temperature and duration varied between samples depending on composition and is discussed further below. Samples were all silver-metallic in appearance, stable in air over a time-scale of months and extremely brittle.

Powder diffraction data on both as cast and annealed material were collected on a SCINTAG  $\theta/2\theta$  Diffractometer using  $\text{Cu K}\alpha_1$  radiation and  $\text{Al}_2\text{O}_3$  as an internal standard. Powder diffraction patterns were indexed using the program TREOR90 [16] and the lattice parameters obtained thereby were refined by a least-squares technique. Single crystal diffraction data on  $\text{Ce}_2\text{CoSi}_3$  were collected on a Rigaku AFC7R diffractometer using graphite monochromated  $\text{Mo K}\alpha$  radiation from a 12kW rotating anode source and again on a P4 automatic 4-circle diffractometer with a sealed tube source (stationary anode) and graphite monochromated  $\text{Mo K}\alpha$  radiation. Magnetic susceptibility data were collected by the Faraday technique and fit to a Curie-Weiss expression, when appropriate, as described elsewhere [17]. Resistance data were obtained by a 4-probe technique. Specific heat measurements on  $\text{Ce}_2\text{CoSi}_3$  were performed by a time constant technique [18].

## Results and Discussion

### *Structural Behavior*

Before commencing the alloy study, we attempted to prepare the Pd and Au containing end members. The powder diffraction pattern for as cast  $\text{Ce}_2\text{PdSi}_3$  could be indexed on a hexagonal cell with  $a = 4.131\text{\AA}$  and  $c = 4.283\text{\AA}$ . After annealing for 2 weeks (one sample) or 5 weeks (second sample) at  $750^\circ\text{C}$ , several small peaks appeared which could be indexed on a hexagonal cell with twice the as cast  $a$  and four times the as cast  $c$ . This suggests that annealed  $\text{Ce}_2\text{PdSi}_3$  may be a new ordered variant ( $2a$ ,  $4c$ ) of the  $\text{AlB}_2$  structure type (Table 1). The powder diffraction patterns of as cast samples of composition " $\text{Ce}_2\text{AuSi}_3$ " could be readily indexed to a tetragonal cell with  $a = 4.222\text{\AA}$  and  $c = 14.375\text{\AA}$  but such samples always became two-phase with a hexagonal phase (Table 2) dominant after anneal at temperatures varying from  $750^\circ\text{C}$  to  $1100^\circ\text{C}$ . For these temperatures, the 2:1:3 composition in the Ce-Au-Si system appears to lie between two solid solution regions: one tetragonal (approaching  $\text{CeSi}_2$ ), the other hexagonal.

Tables 1 and 2 summarise the results of powder X-ray diffraction pattern analyses for samples containing 3d/Pd alloying and 3d/Au alloying, respectively, in  $\text{Ce}_2(3\text{d}/\text{M})\text{Si}_3$ . Annealing of nickel-containing samples was done at  $750^\circ\text{C}$  for 5 weeks. A shorter anneal time of 2 weeks was used for all other samples by increasing the anneal temperature to  $900^\circ\text{C}$ . It was necessary to anneal gold-rich Co/Au compositions an additional 2 weeks at  $900^\circ\text{C}$  to minimize the amount of second phase present in the powder diffraction pattern. Estimates of second phase content are given as the ratio of the most intense unindexed diffraction peak to the most intense indexed peak, expressed as a percentage. For samples that appeared tetragonal as cast and hexagonal after anneal, the major peak from the residual tetragonal phase overlaps the major peak of the hexagonal phase. In this case, the impurity content was estimated from lesser peaks in the powder diffraction patterns.

Both nickel and cobalt appear to form complete solid solutions with palladium in a  $\text{Ce}_2\text{TSi}_3$  composition (Fig. 2) and extensive solid solutions with Au (Fig. 3). The earlier 3d transition elements do not form solid solutions over as broad a range. From Table 1, however, we note that there are still some phases present in the powder diffraction patterns for the earlier 3d element substitutions with unit cells similar to the nickel and cobalt substitutions. The lattice parameters for these phases do change on increasing 3d content. For the cell parameters and impurity phase content in the powder diffraction data to keep changing with increasing substitution, there must be some solid solution region in the quaternary phase diagrams. The  $\text{Ce}_2\text{M}_x\text{Pd}_{1-x}\text{Si}_3$  composition may lie within the boundary of such a region in a palladium rich section but, for increasing  $x$ , the  $\text{Ce}_2\text{M}_x\text{Pd}_{1-x}\text{Si}_3$  composition may exit the single-phase region. Provided that the terminus of the region has not been passed, then the observed  $\text{AlB}_2$ -related (defect) phases must exist on the boundary and change, after anneal, as the overall composition changes.

Upon observing hexagonal cells for cobalt rich  $\text{Ce}_2\text{Co}_x(\text{Pd,Au})_{1-x}\text{Si}_3$  compositions that suggest a  $2a,c$  variant of the  $\text{AlB}_2$  structure, the structure of the cobalt parent,  $\text{Ce}_2\text{CoSi}_3$ , was re-examined. Initial reports [10] on this material gave an  $\text{AlB}_2$  cell with Co and Si disordered on the boron positions. The (1 0 0) and (1 1 0) were the strongest observed superlattice peaks, being approximately 6% of the intensity of the most intense (2 0 1) diffraction peak in  $\text{Ce}_2\text{Co}_{0.5}\text{Au}_{0.5}\text{Si}_3$ . By following the positions of these and other superlattice peaks in powder diffraction with increasing cobalt content, weak peaks in the powder diffraction pattern of  $\text{Ce}_2\text{CoSi}_3$  could be identified near the 1% relative intensity level consistent with a doubling of the  $a$  lattice parameter of the reported cell. Such weak peaks could have easily been missed in earlier studies of  $\text{Ce}_2\text{CoSi}_3$  [10, 15] if samples were not annealed sufficiently or if low signal-to-noise ratios were present. A single crystal study was pursued to examine the structure further.

Shards isolated from a crushed bead of composition  $\text{Ce}_2\text{CoSi}_3$  were examined on a Rigaku AFC7R diffractometer using a 12kW rotating anode source until a crystal suitable for study was found. Data collected on this instrument and crystal could be solved and refined to a  $wR_2$  of 1.6% but with a GooF of 3.18 and non-positive definite cerium thermal parameters. This was unsatisfactory, and was attributed to an absorption correction problem. A further data set was collected on a P4 automatic 4-circle diffractometer. The absorption correction was done by psi-scan methods on this dataset. The structural solution from this dataset was acceptable, with the thermal parameters of all atoms positive definite.

The choice of Laue class based on the *Laue* routine in the XSCANS [19] software used in data collection on the P4 was 6/mmm. Analysis using the program XPREP [20], however, suggested possible space groups of P-3m1 and P6/mmm. Solutions in both space groups were examined but yielded similar results, as discussed below. A final choice of the higher symmetry P6/mmm (No. 191) space group was made after comparing the two refinements.

Starting atomic positions were determined using the programs SIR92 [21] and XS [20]. The SIR92 program would refine in P-3m1 with a residual of 3.5% but would not refine in P6/mmm below 60%. No difficulty was encountered using the XS program to determine starting atomic positions. Subsequent refinement of positions and thermal parameters was done using the program XL [20] with anisotropic thermal parameters for all atoms. The difference made by choice of space group (P-3m1 versus P6/mmm) occurs in the  $z$  atomic positions for Co and Si. In P-3m1,  $z_{\text{Si}}$  was 0.5004(5) and  $z_{\text{Co}}$  was 0.4998(3). Within error, these values are equivalent to  $z = 0.5$  obtained using P6/mmm, hence the choice of P6/mmm. Residuals for all data in P-3m1 were  $R_1 = 0.0334$  and  $wR_2 = 0.0554$  and the GooF was 1.278. These residuals are slightly higher than for P6/mmm (Table 3) and the GooF is slightly lower. Some ambiguity in the choice of spacegroup may remain, however, due to the weak nature of the superlattice reflections. A final difference Fourier synthesis in P6/mmm revealed no significant residual

peaks greater than  $+0.634$  or  $-0.705$   $e/\text{\AA}^3$ . Details of the single crystal data collection and structure refinement in  $P6/mmm$  are given in Table 3. Refined atomic positions for space group  $P6/mmm$  are listed in Table 4. Interatomic distances from the single crystal refinement are given in Table 5.

The structure of  $\text{Ce}_2\text{CoSi}_3$  is indeed related to the  $\text{U}_2\text{RuSi}_3$  type [8] as a  $2a,c$  variant on the  $\text{AlB}_2$  structure type (Fig. 4). Cobalt and silicon form ordered two-dimensional hexagonal networks separated by cerium. In the report on the prototype  $\text{U}_2\text{RuSi}_3$  structure, the silicon atoms (half) occupy a split position ( $12o$ ,  $x = 0.166$ ,  $y = 2x$ ,  $z = 0.4432$ ) but in  $\text{Ce}_2\text{CoSi}_3$ , the silicon atoms are coplanar with the cobalt atoms. Silicon-silicon and cobalt-silicon distances in  $\text{Ce}_2\text{CoSi}_3$  (Table 5), at  $2.387\text{\AA}$  and  $2.292\text{\AA}$ , are comparable to Si-Si and T-Si distances in  $\text{Er}_2\text{RhSi}_3$  [5] ( $d_{\text{Si-Si}} = 2.345\text{\AA}$ ,  $d_{\text{Rh-Si}} = 2.351\text{\AA}$ ). The Si-Si distance is also comparable to that in  $\alpha$ -Si,  $2.352\text{\AA}$  [22], while the Co-Si distance is comparable to the sum of the respective covalent radii,  $2.27\text{\AA}$  [23]. These distances are also comparable to those in  $\text{CeCoSi}_2$  ( $d_{\text{Co-Si}} = 2.29\text{\AA} - 2.34\text{\AA}$ ,  $d_{\text{Si-Si}} \geq 2.44\text{\AA}$ ) [24-26]. Cerium-near neighbour distances in  $\text{Ce}_2\text{CoSi}_3$  are comparable to or slightly larger than those in  $\text{CeCoSi}_2$ . Cerium-silicon distances are  $3.178\text{\AA}$  (Ce1-Si) and  $3.125\text{\AA}$  (Ce2-Si), compared to a range from  $3.07\text{\AA}$  to  $3.19\text{\AA}$  in  $\text{CeCoSi}_2$ . The Ce2-Co distance is  $3.143\text{\AA}$  and slightly larger than the cerium-cobalt distance in  $\text{CeCoSi}_2$  ( $3.12\text{\AA}$ ).

### *Magnetic and Electric Behavior*

The magnetic susceptibilities for select compositions were examined as a function of temperature. In particular, the magnetic behavior of the substitutions involving cobalt were examined since the variations in cell volume as a function of cobalt content (Figs. 2, 3) for both  $\text{Ce}_2\text{Co}_x\text{Pd}_{1-x}\text{Si}_3$  and  $\text{Ce}_2\text{Co}_x\text{Au}_{1-x}\text{Si}_3$  exhibit deviations from linearity for high cobalt content.

This suggests a possible loss or reduction in the cerium moment for the cobalt-rich compositions. Table 6 lists the magnetic data for the compositions examined.

For  $\text{Ce}_2\text{PdSi}_3$ , the inverse magnetic susceptibility (Fig. 5) was measured on ground material (powder). We have previously [17] measured ground material and observed re-orientation of the powder on cooling from the action (torque) of an applied field on an anisotropic magnetic moment. We have done so here as well to obtain a qualitative estimate of the anisotropy in the cerium moment in these silicide materials. This re-orientation usually manifests as a discontinuity in the cooling data, with the orientation of the powder remaining fixed on warming, as observed at 24K in the inset to Figure 5. Since the starting material was polycrystalline, complete orientation of all single crystal grains is not assured, however, the anisotropy appears to be small. Fitting the susceptibility data collected on warming above 100K yields an effective moment per cerium of  $2.48(2)\mu_B$ , consistent with a free ion value of  $2.54\mu_B$ , and a  $\theta$  of 7(1)K, suggesting weak ferromagnetic exchange.

Below 10K, the inverse susceptibility versus temperature decreases in slope and appears to almost plateau by 4.2K with  $\chi^{-1}$  approximately 7.15 mole Ce/emu. This may indicate some ordered magnetic state. At 4.2K and an applied field of 10.1kG, we calculate an ordered moment of  $0.25\mu_B$  per Ce. This is much reduced from a moment calculated from the product of the Landé factor,  $g$  (6/7), and angular momentum,  $J$  (5/2), for Ce ( $gJ = 2.21\mu_B$ ) or for a crystal field split cerium moment ( $0.7\mu_B$  and  $1.3\mu_B$  being typical measured values). At 4.2K then,  $\text{Ce}_2\text{PdSi}_3$  is not likely to be a completely ordered ferromagnetic material. It may be that 4.2K is not sufficiently far below  $T_C$  to give the maximum moment, or perhaps some more complicated spin structure is present.

The resistivity of  $\text{Ce}_2\text{PdSi}_3$  is shown in Figure 6 as a function of temperature from 4.2K to 300K. Some hysteresis on warming is evident and may be due to contact problems or some gradual change in contact between grain boundaries. These silicide materials are all brittle

intermetallics and observations of cracks on the surfaces of arc-melted beads often indicate the presence of some cracks within the material. No large discontinuities are present in the resistivity to suggest continued cracking on cooling in this sample. It would be prudent, however, to interpret the magnitude of the resistivity as only an upper limit on the absolute value. The overall behavior is that of a metallic system with a decrease in resistivity below 100K corresponding to a decrease in magnetic scattering from thermally depopulating crystal-field-split cerium 4f states. A decrease in resistivity is also apparent below 10K, coincident with the noted behavior in the susceptibility.

The temperature dependent inverse magnetic susceptibilities for the other materials listed in Table 6 are given in Figure 7 for Pd- and Ni- containing materials and in Figure 8 for Co/Au alloy samples. The behavior of  $\text{Ce}_2\text{NiSi}_3$  is consistent with that previously reported [15] with an effective high temperature moment of  $2.48(1)\mu_B$  per cerium and  $\theta$  of  $-22(2)\text{K}$  compared to the reported moment of  $2.46\mu_B$  and  $\theta$  of  $-18\text{K}$ . The behavior of the cobalt containing compounds is more complicated.

While the temperature dependence of the magnetic susceptibility of the cobalt-substituted materials can be fit to a Curie-Weiss expression, it may be inappropriate to do so for the more cobalt-rich samples. With increasing cobalt content, we observe an increase in  $\chi^{-1}$  corresponding to a decrease in magnetisation. There is still some roughly linear dependence of the inverse susceptibility on temperature above 100K for most samples (perhaps above 250K for  $\text{Ce}_2\text{CoSi}_3$ ), but the increasingly negative  $\theta$  (Table 6) values most likely do not result from anti-ferromagnetic interactions. Most of these cobalt-containing materials exhibit large increases in magnetisation below 100K. The exception is the cobalt end-member which plateaus below 80K and has what may be a small Curie tail from small amounts ( $<1\%$ ) of impurities not observed in powder diffraction data. A small deviation near 5K in this tail may indicate ordering in this possible second phase. It may also be possible for some cerium moments in  $\text{Ce}_2\text{CoSi}_3$  to be present, as

will be discussed below. The ternary compounds CeRhIn [27] and Ce<sub>2</sub>Ni<sub>3</sub>Si<sub>5</sub> [28] exhibit similar behavior in their susceptibilities (plateauing at low temperature, non-magnetic behavior). The resistivities of these two materials are also similar in temperature dependence to that for Ce<sub>2</sub>CoSi<sub>3</sub> (Fig. 9) with a roughly flat region at high temperature and broad decrease on cooling. In [27] and [28], this type of behavior was attributed to interconfiguration fluctuations (ICF) of the cerium as described by Hirst [29] and Sales et al. [30]. Both CeCoSi<sub>2</sub> [27] and CeCoSi<sub>3</sub> [31] exhibit Pauli paramagnetic behavior with some weak temperature dependence that has also been described, in the case of CeCoSi<sub>3</sub>, as spin fluctuations in an ICF model [31].

Specific heat data below 20K were collected on Ce<sub>2</sub>CoSi<sub>3</sub> and are plotted as  $C/T$  versus  $T^2$  in Figure 10. The behavior of  $C/T$  above 10K is roughly linear and extrapolates to a  $C/T$  value at  $T = 0$  K of  $\gamma = 59.7 \text{ mJ/mol-Ce} \cdot \text{K}^2$ . The actual data deviates from linearity below 10K. A small feature near 5K is also present, as in the susceptibility. The data below this feature tend toward an intercept of  $71.5 \text{ mJ/mol-Ce} \cdot \text{K}^2$ . Both of the values are comparable to other valence fluctuation materials [28].

When discussing the trend in magnetic behavior in the series U<sub>2</sub>TSi<sub>3</sub>, in particular with T one of Fe, Ru or Os, Chevalier et al. [32] considered the interaction between the  $nd$  orbitals on the transition element with the  $5f$  orbitals on uranium. Given that the  $4f$  orbitals of cerium are more localised than the  $5f$  orbitals of uranium, we consider an alternate interpretation of the magnetic behavior in the series Ce<sub>2</sub>TSi<sub>3</sub>. In changing structure from CeCoSi<sub>3</sub> [31] (ordered BaAl<sub>4</sub> type, variant BaNiSn<sub>3</sub>) to CeCoSi<sub>2</sub> (CeNiSi<sub>2</sub> type described as alternating BaAl<sub>4</sub> and AlB<sub>2</sub> [25]) to Ce<sub>2</sub>CoSi<sub>3</sub> (ordered AlB<sub>2</sub>), the cerium-silicon near neighbour distances increase from a range of 3.01Å - 3.16Å in CeCoSi<sub>3</sub> through a range of 3.07Å-3.19Å in CeCoSi<sub>2</sub> to a range of 3.125Å-3.178Å in Ce<sub>2</sub>CoSi<sub>3</sub>. The cerium-cobalt distances vary from 3.28Å to 3.12Å to 3.14Å, respectively, decreasing, but not as steadily as the increase in the minimum cerium-silicon distances. The average near-neighbour distance does appear to be increasing. Overlap of orbitals

on near-neighbour atoms with cerium orbitals and cerium 5d orbitals in particular will depend on the cerium-near neighbour distance and geometry and may lead to a band near the Fermi level with appreciable cerium 5d character if strong overlap is present. If additional stabilisation energy of the material can be achieved by promoting the 4f electron on each cerium into this band (i.e. if the effective energy of the  $6s^2 5d^2 4f^0$  band state becomes lower than that of the  $6s^2 5d^1 4f^1$  state with localised f-electron and delocalised d-electron), then the cerium atoms will have non-magnetic ground states. If the energies of the two configurations are not too disparate, then the electron may hop between the two states (interconfiguration fluctuations [33]). As the cerium-near neighbour distance is increased in going from  $\text{CeCoSi}_3$  to  $\text{Ce}_2\text{CoSi}_3$  - in essence, this is the opposite of applying pressure - we decrease the overlap with the cerium 5d orbitals. This would decrease the 3p-5d bandwidth and raise the effective energy of the  $5d^2 4f^0$  electrons, decreasing the effective separation between the d electrons and  $5d^1 4f^1$  states on each cerium.

In  $\text{Ce}_2\text{CoSi}_3$ , the ground state is still non-magnetic, but the energy separation between the two states ( $5d^2$  and  $5d^1 4f^1$ ) in this model would be small. We must also consider the effect of having two crystallographically distinct cerium sites (Table 5). At the corners of the unit cell (Fig. 4), the Ce1 atoms are co-ordinated by 12 silicon atoms all at a distance of 3.178Å. Three-quarters of the cerium atoms in the unit cell are Ce2, however, and are co-ordinated at shorter distances by 8 Si ( $d_{\text{Ce2-Si}} = 3.125\text{Å}$ ) and 4 Co ( $d_{\text{Ce2-Co}} = 3.143\text{Å}$ ). This could lead to different and perhaps weaker interactions for Ce1. It is possible that the low temperature "tail" in the susceptibility is a reflection of having 1/4 of the cerium atoms in  $\text{Ce}_2\text{CoSi}_3$  with a weakly magnetic ground state (perhaps with some Ce1-Ce1 exchange interaction perpendicular to the hexagonal layers leading to magnetic ordering near 5K). Such speculation, however, suggests that further study of  $\text{Ce}_2\text{CoSi}_3$  at low temperatures is required.

Upon substituting the larger transition elements Pd and Au, the Ce-Si distances increase (obvious from increased *a* and *c* lattice parameters, Tables 1 and 2), the valence electron count

increases, and disorder is induced in the Ce2 environment. Increased separation and electron count will lead to less overlap and a narrowing and greater filling of any band based on this overlap. Disorder in the Ce2 environment could lead to magnetically inequivalent ground states for individual Ce2 atoms, depending on type and number of each transition element near-neighbour, similar to the discussion above for Ce1 versus Ce2. The net effect is an increase in magnetisation as the cobalt content decreases, particularly at low temperature as magnetic ground states become favoured. There is a corresponding decrease in spin fluctuations as the magnetic ground state becomes more favoured. This is reflected in the decreasing magnitude of the  $\theta$  values (Table 6) and the apparent return to well-developed  $4f^1$  cerium behavior for  $x \leq 0.5$  in  $\text{Ce}_2\text{Co}_x(\text{Pd or Au})_{1-x}\text{Si}_3$ .

## Conclusions

Limited flexibility in substitution does exist in  $\text{Ce}_2\text{TSi}_3$  but is more extensive for the later transition elements Co and Ni when alloying with Pd or Au than for the earlier 3d elements Cr, Mn and Fe. In particular, extensive substitution can be done between Co and Pd or Au in  $\text{Ce}_2\text{CoSi}_3$ . The structure of  $\text{Ce}_2\text{CoSi}_3$  was re-examined and found to an ordered variant of the  $\text{AlB}_2$  structure. A transition from valent fluctuating to trivalent cerium behavior is observed with decreasing cobalt content in  $\text{Ce}_2\text{Co}_x(\text{Pd or Au})_{1-x}\text{Si}_3$ . This was attributed to decreasing Ce-Si interactions as the incorporation of the larger transition element increased the lattice spacings and hence the Ce-Si distances.

## Acknowledgements

This work was supported by the Office of Naval Research. Specific heat measurements on  $\text{Ce}_2\text{CoSi}_3$  were performed in collaboration with J.S. Kim and G.R. Stewart at the University of Florida (Gainesville). We would like to thank R.C. Haushalter for access to the Rigaku

diffractometer at the NEC Research Institute and A. Simon for access to the facilities at the MPI. We are also grateful to N.E. Brese for valuable discussions.

## References

- [1.] P. Villars and L.D. Calvert, *Pearson's Handbook of Crystallographic Data for Intermetallic Phases*, ASM International, Materials Park, 1991.
- [2.] J.G. Sereni and O. Trovarelli, *J. Magn. Magn. Mater.*, 140-144 (1995) 885.
- [3.] B. Chevalier, P. LeJay, J. Etourneau and P. Hagenmuller, *Solid State Comm.*, 49 (1984) 753.
- [4.] P. Kotsanidis, J.K. Yakinthos and E. Gamari-Seale, *J. Magn. Magn. Mater.*, 87 (1990) 199.
- [5.] R.E. Gladyshevskii, K. Cenxual and E. Parthé, *J. Alloys Comp.*, 189 (1992) 221.
- [6.] J.H. Albering, R. Pöttgen, W. Jeitschko, R.-D. Hoffmann, B. Chevalier and J. Etourneau, *J. Alloys Comp.*, 206 (1994) 133.
- [7.] R. Pöttgen and D. Kaczorowski, *J. Alloys Comp.*, 201 (1993) 157.
- [8.] R. Pöttgen, P. Gravereau, B. Darriet, B. Chevalier, E. Hickey and J. Etourneau, *J. Mater. Chem.*, 4 (1994) 463.
- [9.] E. Dowty, ATOMS for Windows Version 3.1, Shape Software, Kingsport TN, 1994.
- [10.] O.I. Bodak and E.I. Gladyshevskii, *Izv. Akad. Nauk SSSR, Neorg. Mater.*, 6 (1970) 1186.
- [11.] O.I. Bodak, M.G. Mis'kiv, A.T. Tyvanchuk, O.I. Kharchenko and E.I. Gladyshevskii, *Izv. Akad. Nauk SSSR, Neorg. Mater.*, 9 (1973) 864.
- [12.] O.I. Bodak, Ya.M. Kalychak and E.I. Gladyshevskii, *Inorg. Mater.*, 10 (1974) 388.
- [13.] O.I. Bodak, E.I. Gladyshevskii, A.V. Kardash and E.E. Cherkashin, *Izv. Akad. Nauk, Neorg. Mater.*, 6 (1970) 1069.
- [14.] I. Mayer and M. Tassa, *J. Less-Common Met.*, 19 (1969) 173.
- [15.] S.K. Dhar, R. Balasubramaniam, S.M. Pattalwar and R. Vijayaraghavan, *J. Alloys Comp.*, 210 (1994) 339.
- [16.] P.E. Werner, L. Eriksson and M. Westdahl, *J. Appl. Crystallogr.*, 18 (1985) 367.
- [17.] R.A. Gordon, Y. Ijiri, C.M. Spencer and F.J. DiSalvo, *J. Alloys Comp.*, 224 (1995) 101.
- [18.] J. Kim, *Thesis*, University of Florida, 1992.

- [19.] XSCANS 2.0 - Data Collection Package, Siemens Industrial Automation Inc., 1993&1994.
- [20.] G.M. Sheldrick, SHELXTL PC Version 5.0 - An Integrated System for Solving, Refining and Displaying Crystal Structure from Diffraction Data, Siemens Analytical X-Ray Instruments Inc. Madison, WI, 1994.
- [21.] A. Altomare, G. Cascarano, C. Giacovazzo and A. Guagliardi, *J. Appl. Crystallogr.*, 27 (1994) 435.
- [22.] J. Donohue, *The Structures of the Elements*, Wiley, New York, 1974.
- [23.] R.T. Sanderson, *Inorganic Chemistry*, Reinhold Publishing Corporation, New York, 1967.
- [24.] Distances calculated using the program EUTAX: N.E. Brese and M. O'Keefe, *Acta Cryst.*, B47 (1991) 192, as modified for the DOS environment by N.E. Brese.
- [25.] B. Chabot, E. Parthé and J. Steinmetz, *J. Less-Common Met.*, 125 (1986) 147.
- [26.] M. Pelizzzone, H.F. Braun and J. Muller, *J. Magn. Magn. Mater.*, 30 (1982) 33.
- [27.] D.T. Adroja, S.K. Malik, B.D. Padalia and R. Vijayaraghavan, *Phys. Rev. B*, 39 (1989) 4831.
- [28.] R. Nagarajan, S.K. Dhar, L.C. Gupta, R. Vijayaraghavan and B.D. Padalia, *Phys. Rev. B*, 46 (1992) 9009.
- [29.] L.L. Hirst in: *Magnetism and Magnetic Materials - 1974 (San Francisco)*, C.D. Graham, G.H. Lander and J.J. Rhyne (eds.), AIP, New York, 1975.
- [30.] B.C. Sales and D. Wohlleben, *Phys. Rev. Lett.*, 35 (1975) 1240.
- [31.] B. Rupp, P. Rogl and F. Hulliger, *J. Less-Common Met.*, 135 (1987) 113.
- [32.] B. Chevalier, R. Pöttgen, B. Darriet, P. Gravereau and J. Etourneau, *J. Alloys Comp.*, 233 (1996) 150.
- [33.] J.A. Wilson, *Structure and Bonding*, 32 (1977) 57.

**Table 1**

Cell parameters, reduced  $\text{AlB}_2$  cell volume and the ratio of the largest unindexed peak (estimated if overlapping, see text) to the largest indexed peak (the 2 0 1 peak for the  $2a$ ,  $c$  ordered variant of  $\text{AlB}_2$ ) for  $\text{Ce}_2\text{M}_x\text{Pd}_{1-x}\text{Si}_3$  compositions.

Material	Symmetry	$a/\text{\AA}$	$c/\text{\AA}$	$V/\text{\AA}^3$ (cell)	$V/\text{\AA}^3$ ( $\text{AlB}_2$ )	$I_{\text{imp}}/I_{\text{max}}$ (%)	Ref./ note
$\text{Ce}_2\text{Ni}_x\text{Pd}_{1-x}\text{Si}_3$							
$x = 0$	hex.	8.2631(5)	17.132(2)	1013.0(1)	63.31	--	
$x = 0.2$	"	8.2274(8)	17.118(4)	1003.5(3)	62.72	--	
$x = 0.4$	"	8.1908(7)	17.114(3)	994.3(2)	62.15	--	
$x = 0.6$	hex.	4.0776(4)	4.2816(4)	61.65(1)	61.65	--	
$x = 0.8$	"	4.0589(3)	4.2795(3)	61.06(1)	61.06	--	
$x = 1$	"	4.0406(4)	4.2801(5)	60.52(1)	60.52	--	
$\text{CeNi}_{0.5}\text{Si}_{1.5}$	"	4.048	4.291	60.89	60.89		[14]
$\text{CeNi}_{0.53}\text{Si}_{1.47}$	"	4.039	4.287	60.56	60.56		[10]
$\text{CeNi}_{0.4}\text{Si}_{1.6}$	"	4.034	4.294	60.51	60.51		[13]
$\text{Ce}_2\text{Co}_x\text{Pd}_{1-x}\text{Si}_3$							
$x = 0.2$	hex.	8.2318(9)	4.2709(7)	250.63(6)	62.65	1	
$x = 0.4$	"	8.2009(7)	4.2586(5)	248.04(4)	62.01	< 1	
$x = 0.5$	"	8.1869(5)	4.2494(4)	246.66(3)	61.66	--	
$x = 0.6$	"	8.1714(6)	4.2442(4)	245.42(3)	61.36	--	
$x = 0.8$	"	8.1376(6)	4.2249(4)	242.30(3)	60.57	--	
$x = 0.9$	"	8.1161(7)	4.2100(5)	240.16(4)	60.04	--	
$x = 1.0$	"	8.0967(7)	4.1959(5)	238.22(4)	59.56	--	
$\text{CeCo}_{0.5}\text{Si}_{1.5}$	"	4.044	4.194	59.40	59.40		[9]
$\text{CeCo}_{0.4}\text{Si}_{1.6}$	"	4.046	4.266	60.48	60.48		[13]
$\text{CeCo}_{0.4}\text{Si}_{1.6}$	"	4.055	4.226	60.18	60.18		[14]
$\text{Ce}_2\text{Fe}_x\text{Pd}_{1-x}\text{Si}_3$							
$x = 0.25$	hex.	8.2414(9)	4.2674(7)	251.01(6)	62.75	1	
$x = 0.5$	"	8.2229(9)	4.252(1)	248.96(7)	62.24	4	
$x = 0.75$	"	4.0978(5)	4.2431(5)	61.70(1)	61.70	10	
$x = 1$	"	4.062(2)	4.212(4)	60.19(7)	60.19	26	
$\text{Ce}_2\text{FeSi}_3$	"	4.065	4.191	59.97	59.97		[11]
$\text{CeFe}_{0.4}\text{Si}_{1.6}$	"	4.058	4.265	60.82	60.82		[13]
$\text{CeMn}_x\text{Pd}_{1-x}\text{Si}_3$							
$x = 0.25$	hex.	8.2573(7)	17.113(3)	1010.5(2)	63.16	1	
$x = 0.5$	tetrag.	4.1806(6)	14.294(3)	249.82(7)	[62.5]	4	as cast
$x = 0.5$	hex.	4.1140(7)	4.2700(7)	62.59(1)	62.59	(15)	annealed
$x = 0.75$	tetrag.	4.1804(4)	14.177(2)	247.75(5)	[61.9]	16	annealed
$\text{Ce}_2\text{Cr}_{0.5}\text{Pd}_{0.5}\text{Si}_3$	"	4.1823(8)	14.259(3)	249.41(9)	[62.4]	9	as cast
$\text{Ce}_2\text{Cr}_{0.5}\text{Pd}_{0.5}\text{Si}_3$	hex.	4.1130(4)	4.2779(5)	62.67(1)	62.67	(30)	annealed

**Table 2**

Cell parameters, reduced  $\text{AlB}_2$  cell volume and the ratio of the largest unindexed peak (estimated if overlapping) to the largest indexed peak (the 2 0 1 peak for the  $2a$ ,  $c$  ordered variant of  $\text{AlB}_2$ ) for  $\text{Ce}_2\text{M}_x\text{Au}_{1-x}\text{Si}_3$  compositions.

Material	Symmetry	$a/\text{\AA}$	$c/\text{\AA}$	$V/\text{\AA}^3$ (cell)	$V/\text{\AA}^3$ ( $\text{AlB}_2$ )	$I_{\text{imp}}/I_{\text{max}}$ (%)	Note
<b><math>\text{Ce}_2\text{Ni}_x\text{Au}_{1-x}\text{Si}_3</math></b>							
$x = 0$	tetrag.	4.2224(3)	14.375(1)	256.34(3)	[64.1]	--	as cast
$x = 0$	hex.	8.284(1)	8.701(1)	517.1(1)	64.64	(30)	annealed
$x = 0.1$	"	4.1264(5)	4.3459(6)	64.08(1)	64.08	1	
$x = 0.25$	"	4.1108(5)	4.3373(6)	63.47(1)	63.47	< 1	
$x = 0.5$	"	4.0917(4)	4.3226(6)	62.67(1)	62.67	--	
$x = 0.75$	"	4.0680(4)	4.3034(5)	61.68(1)	61.68	--	
$x = 1$	"	4.0406(4)	4.2801(5)	60.52(1)	60.52	--	
<b><math>\text{Ce}_2\text{Co}_x\text{Au}_{1-x}\text{Si}_3</math></b>							
$x = 0.2$	hex.	8.2408(7)	8.6816(8)	510.59(8)	63.82	1	
$x = 0.4$	"	4.1055(2)	4.3157(4)	63.00(1)	63.00	1	
$x = 0.5$	"	8.1995(8)	4.3028(5)	250.53(5)	62.63	< 1	
$x = 0.6$	"	8.1761(9)	4.2862(5)	248.14(5)	62.03	--	
$x = 0.8$	"	8.1445(7)	4.2479(5)	244.02(4)	61.01	--	
$x = 0.9$	"	8.1180(7)	4.2222(6)	240.97(5)	60.24	--	
$x = 1$	"	8.0967(7)	4.1959(5)	238.22(4)	59.56	--	
<b><math>\text{Ce}_2\text{Fe}_x\text{Au}_{1-x}\text{Si}_3</math></b>							
$x = 0.25$	hex.	4.1232(3)	4.3275(5)	63.71(1)	63.71	< 1	
$x = 0.5$	"	8.2275(7)	4.2965(4)	251.88(4)	62.97	3	
$x = 0.75$	"	8.1953(8)	4.2669(5)	248.19(4)	62.05	8	
$x = 1$	"	4.062(2)	4.212(4)	60.19(7)	60.19	26	
<b><math>\text{Ce}_2\text{Mn}_x\text{Au}_{1-x}\text{Si}_3</math></b>							
$x = 0.5$	tetrag.	4.2031(4)	14.274(1)	252.17(4)	[63.0]	4	annealed
<b><math>\text{Ce}_2\text{Cr}_x\text{Au}_{1-x}\text{Si}_3</math></b>							
$x = 0.5$	tetrag.	4.2087(3)	14.256(1)	252.52(3)	[63.1]	9	annealed

**Table 3**Crystal and structure refinement data for Ce<sub>2</sub>CoSi<sub>3</sub>.

Empirical formula	Ce <sub>2</sub> CoSi <sub>3</sub>
Formula weight	423.44
Temperature	293(2) K
Wavelength	0.71069 Å
Crystal system	Hexagonal
Space group	P6/mmm (No. 191)
Unit cell dimensions	a = 8.104(2) Å c = 4.197(2) Å
Volume, Formula units	238.7(1) Å <sup>3</sup> , 2
Density (calculated)	5.891 g/cm <sup>3</sup>
Absorption co-efficient	22.738 mm <sup>-1</sup>
F(000)	370
Crystal size	0.10 x 0.10 x 0.05 mm <sup>3</sup>
Theta range for data collection	2.90° to 29.91°
Limiting indices	-3 ≤ h ≤ 7, -5 ≤ k ≤ 9, -5 ≤ l ≤ 5
Reflections collected	1398
Independent reflections	172 [R <sub>int</sub> = 0.0494]
Reflections with I > 2σ(I)	142 [R <sub>σ</sub> = 0.0309]
Absorption correction	From ψ-scan data
Max. and min. transmission	0.624 and 0.450
Refinement method	Full-matrix least-squares on F <sup>2</sup>
Data / restraints / parameters	172 / 0 / 13
Goodness-of-fit on F <sup>2</sup>	1.457
Final R indices [I > 2σ(I)]	R1 = 0.0218, wR2 = 0.0463
R indices (all data)	R1 = 0.0272, wR2 = 0.0484
Extinction coefficient	0.0072(6)
Largest diff. peak and hole	0.634 and -0.705 e/Å <sup>3</sup>

**Table 4**

Atomic co-ordinates and isotropic displacement parameters ( $\text{pm}^2$ ) for  $\text{Ce}_2\text{CoSi}_3$  with  $U_{\text{eq}}$  defined as one third of the trace of the diagonalised  $U_{ij}$  tensor.

Atom	Wyckoff Site	x	y	z	$U_{\text{eq}}$
Ce(1)	1a	0	0	0	47(3)
Ce(2)	3f	0.5	0	0	56(2)
Co	2d	1/3	2/3	0.5	114(4)
Si	6m	0.1702(1)	0.3403(2)	0.5	67(5)

**Table 5**

Interatomic distances in  $\text{Ce}_2\text{CoSi}_3$  up to 3.5Å for Ce-Co, Ce-Si, Co-Si and Si-Si distances and 4.2Å for Ce-Ce distances. Standard deviations are all 0.002Å or less.

Ce1:	12 Si	3.178	Ce2:	8 Si	3.125	Si:	1 Co	2.292
	6 Ce2	4.052		4 Co	3.143		2 Si	2.387
	2 Ce1	4.197		2 Ce1	4.052		4 Ce	3.125
				4 Ce2	4.052		2 Ce	3.178
Co:	3 Si	2.292		2 Ce2	4.197			
	6 Ce2	3.143						

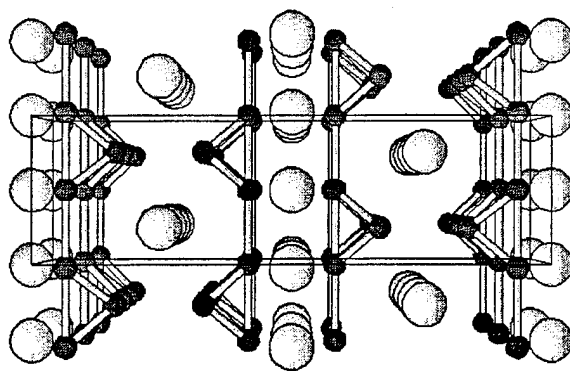
**Table 6**

Summary of magnetic data on  $\text{Ce}_2\text{TSi}_3$  (T = transition metals) materials examined by magnetic susceptibility.

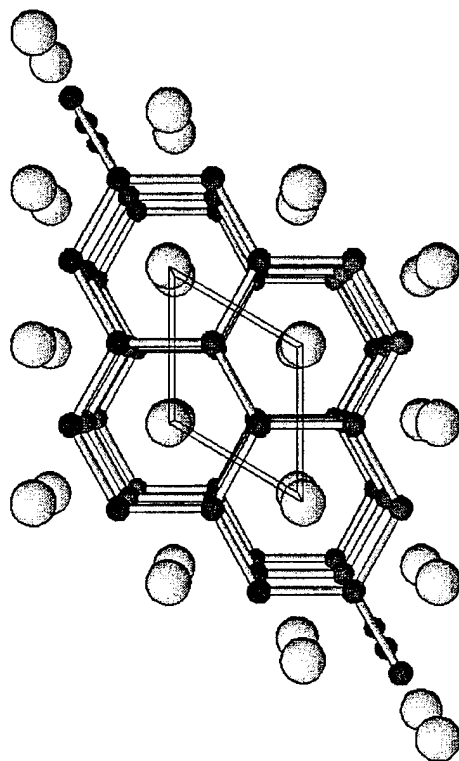
Material	fit range/K	$\mu/\mu_B$	$\theta/\text{K}$	$\chi_0$ ( $10^{-3}$ emu/mol Ce)
$\text{Ce}_2\text{Co}_x\text{Pd}_{1-x}\text{Si}_3$				
x = 0	100-300	2.48(2)	7(1)	0.13(5)
x = 0.5	70-320	2.46(3)	-32(2)	0.21(4)
x = 0.8	100-300	2.50(2)	-82(2)	0.24(4)
$\text{Ce}_2\text{NiSi}_3$	80-300	2.48(1)	-22(2)	0.19(5)
$\text{Ce}_2\text{Co}_x\text{Au}_{1-x}\text{Si}_3$				
x = 0.2	80-315	2.48(2)	-5(2)	0.08(6)
x = 0.5	80-320	2.44(1)	-9(1)	0.18(5)
x = 0.6	80-320	2.42(5)	-16(4)	0.23(6)
x = 0.8	80-300	2.35(4)	-42(4)	0.36(7)
x = 0.9	80-340	2.45(11)	-107(13)	0.3(1)

## Figure Captions

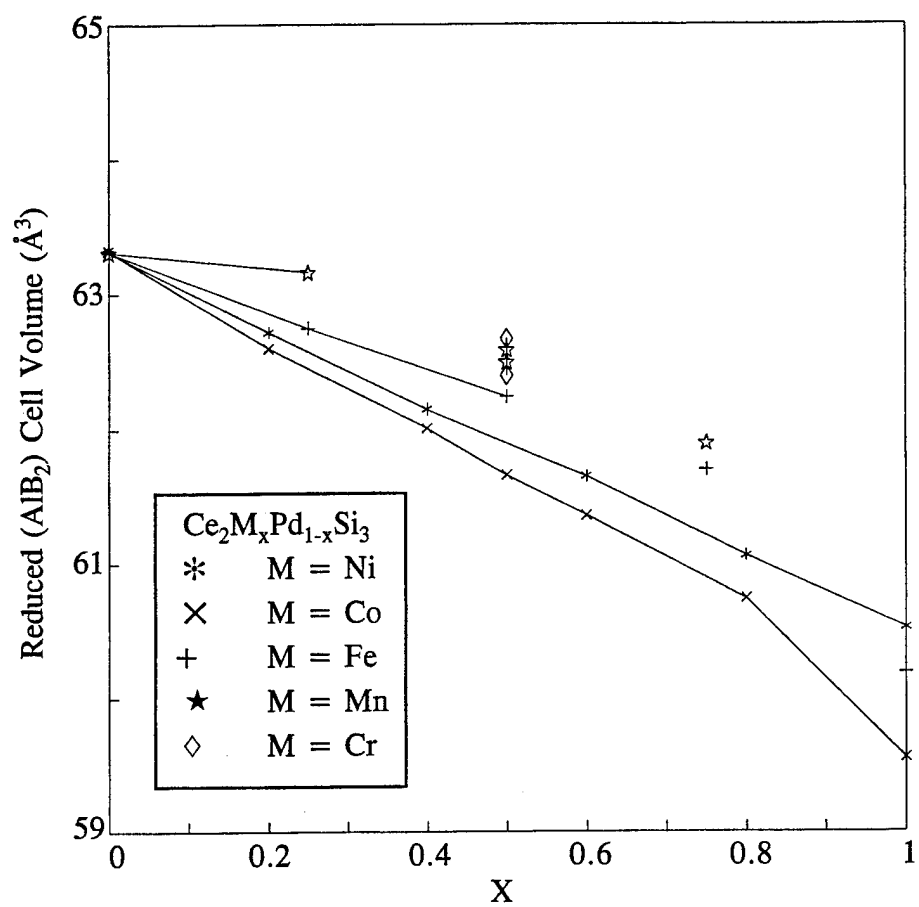
- Figure 1. Perspective views [9] of the structures of (a)  $\alpha$ -ThSi<sub>2</sub> and (b)  $\beta$ -ThSi<sub>2</sub>, also called the AlB<sub>2</sub> structure type. Large white spheres are Th and the small, grey spheres are Si.
- Figure 2. Dependence of reduced AlB<sub>2</sub> cell volume on M = 3d transition element content for Ce<sub>2</sub>M<sub>x</sub>Pd<sub>1-x</sub>Si<sub>3</sub> compositions. Lines connect compositions with less than 10% estimated impurity content.
- Figure 3. Dependence of reduced AlB<sub>2</sub> cell volume on M = 3d transition element content in Ce<sub>2</sub>M<sub>x</sub>Au<sub>1-x</sub>Si<sub>3</sub> compositions. Lines connect compositions with less than 10% estimated impurity content.
- Figure 4. Perspective view of the unit cell of Ce<sub>2</sub>CoSi<sub>3</sub> with adjoining atoms in the CoSi<sub>3</sub> network. Lighter large spheres are cerium atoms marking the corners of the unit cell. Dark medium spheres in the network are cobalt atoms.
- Figure 5. Inverse magnetic susceptibility of Ce<sub>2</sub>PdSi<sub>3</sub> from 4.2K to 300K.
- Figure 6. Resistivity of Ce<sub>2</sub>PdSi<sub>3</sub> from 4.2K to 300K.
- Figure 7. Temperature dependence of the inverse magnetic susceptibilities for several Ce<sub>2</sub>Co<sub>x</sub>Pd<sub>1-x</sub>Si<sub>3</sub> compositions and Ce<sub>2</sub>NiSi<sub>3</sub>.
- Figure 8. Temperature dependence of the inverse magnetic susceptibilities of Ce<sub>2</sub>Co<sub>x</sub>Au<sub>1-x</sub>Si<sub>3</sub> compositions.
- Figure 9. Temperature dependence of the resistance of Ce<sub>2</sub>CoSi<sub>3</sub>. Cracks in the sample prevent determination of an absolute resistivity.
- Figure 10. Specific heat divided by temperature as a function of the square of the temperature from 1.178K to 20K.

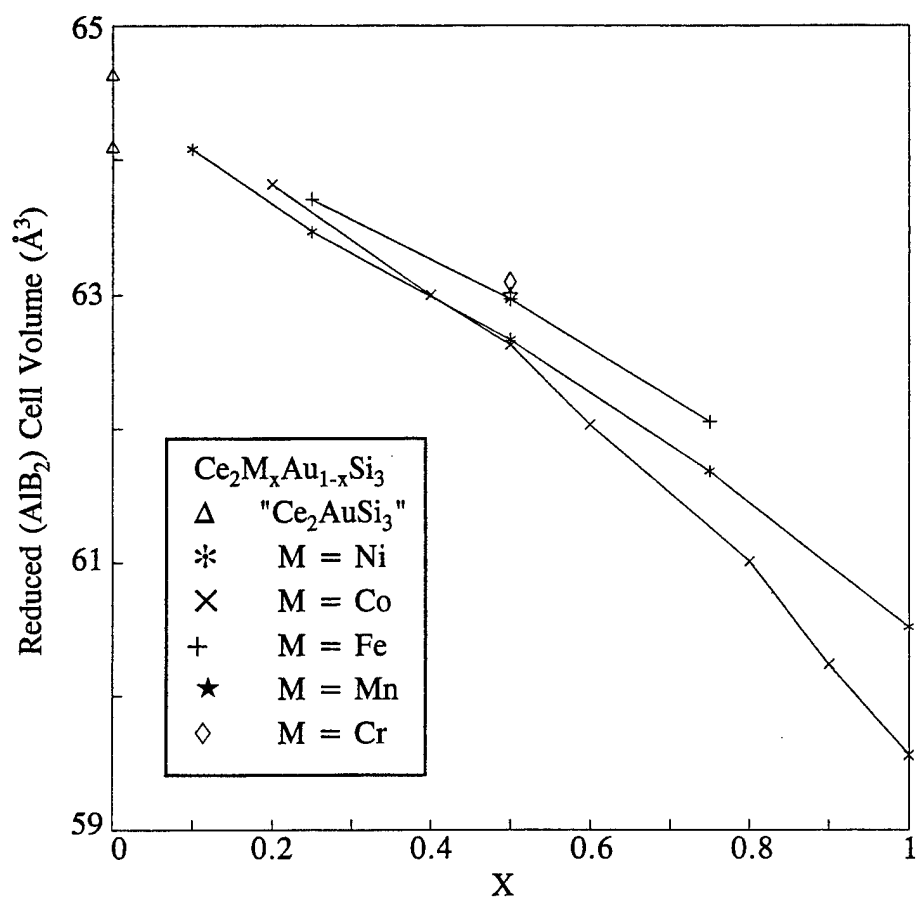


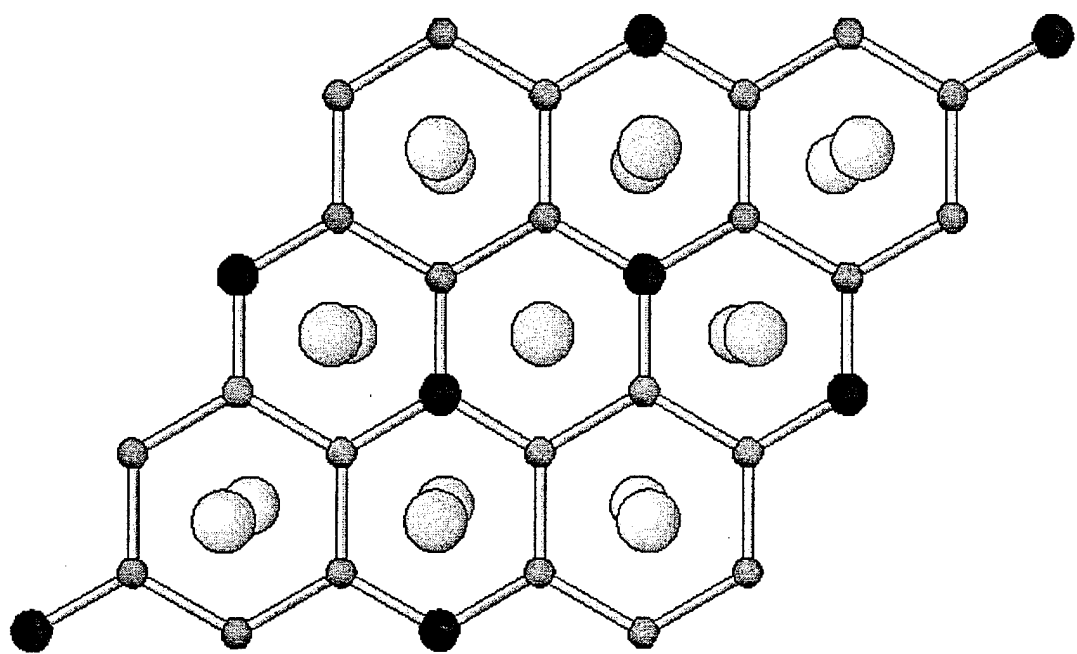
(a)  $\alpha$ -ThSi<sub>2</sub>

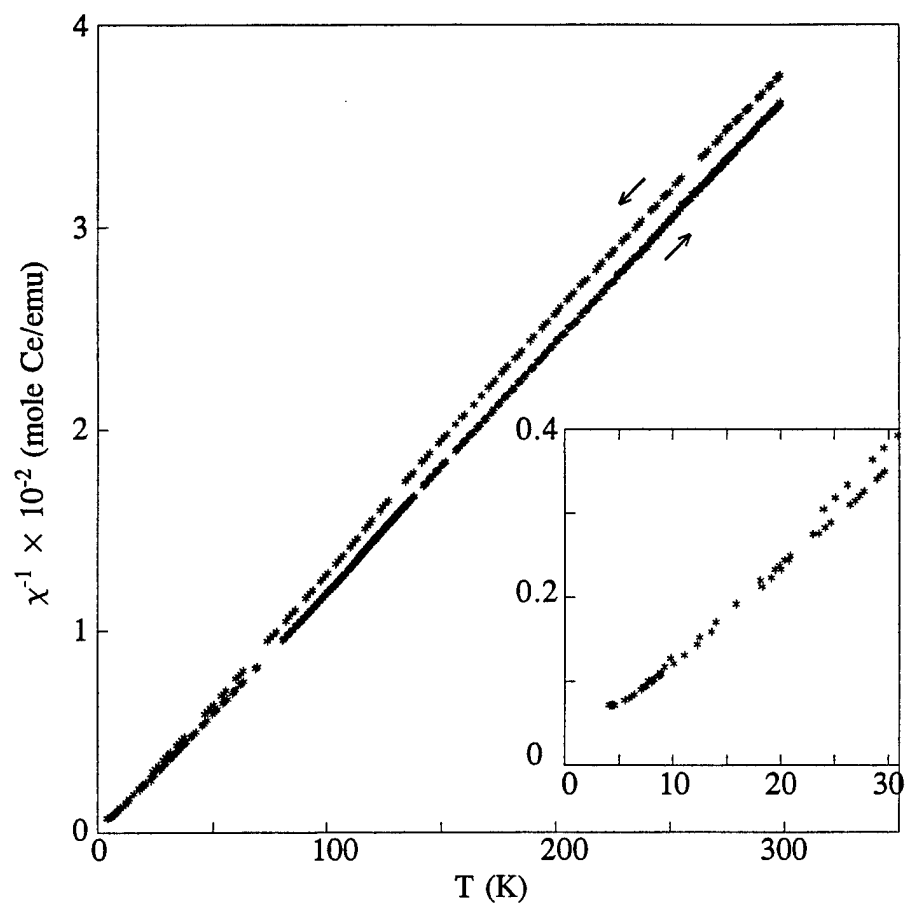


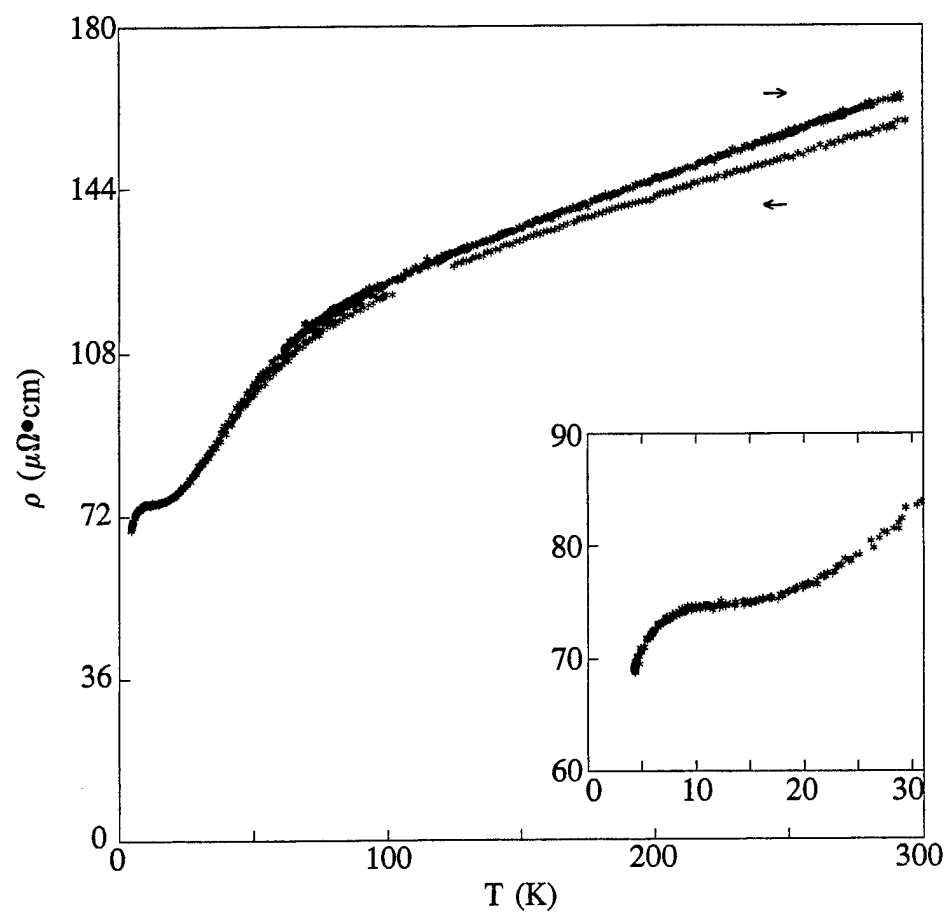
(b)  $\beta$ -ThSi<sub>2</sub> (AlB<sub>2</sub>)

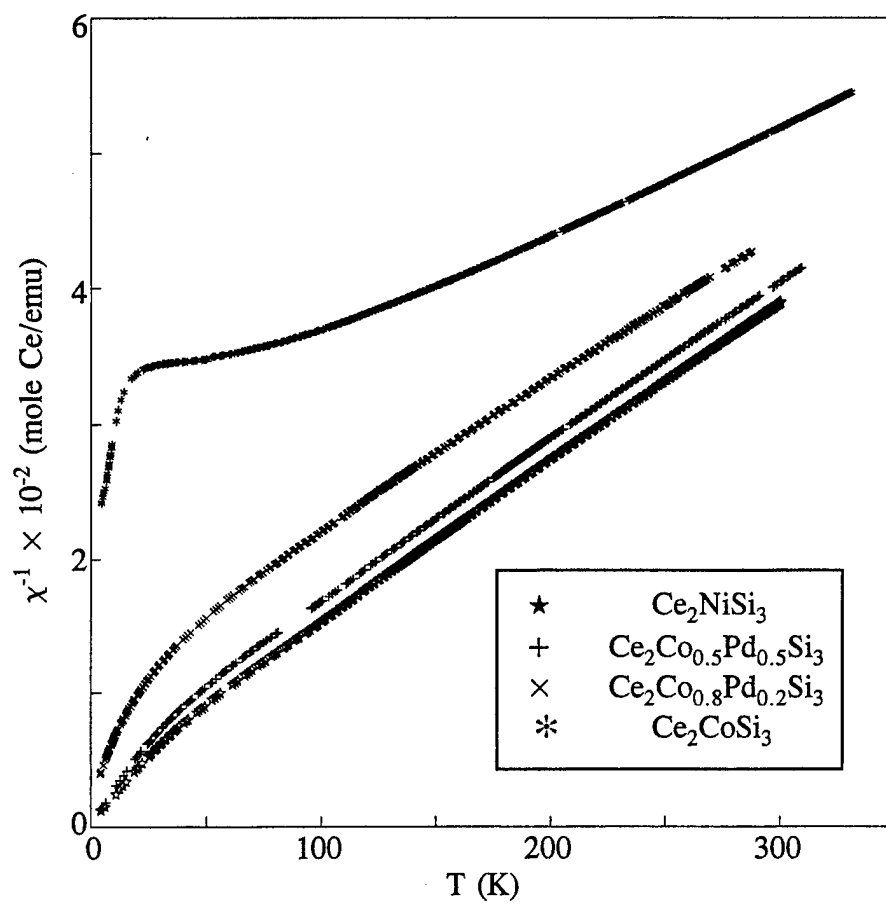


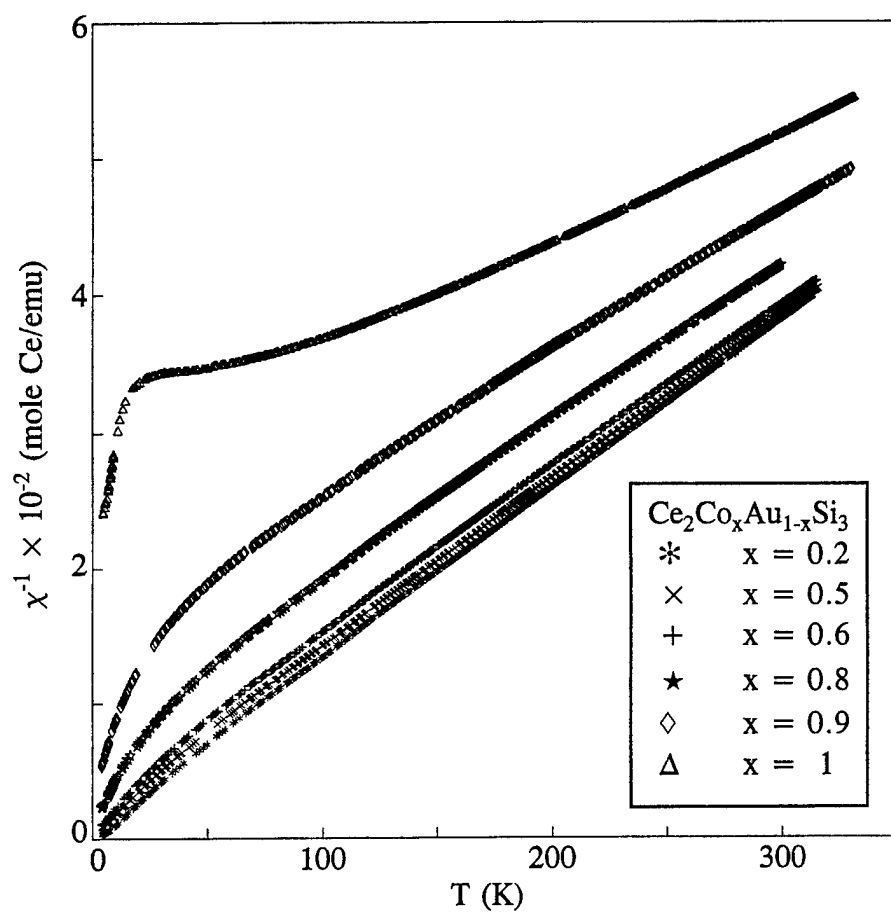


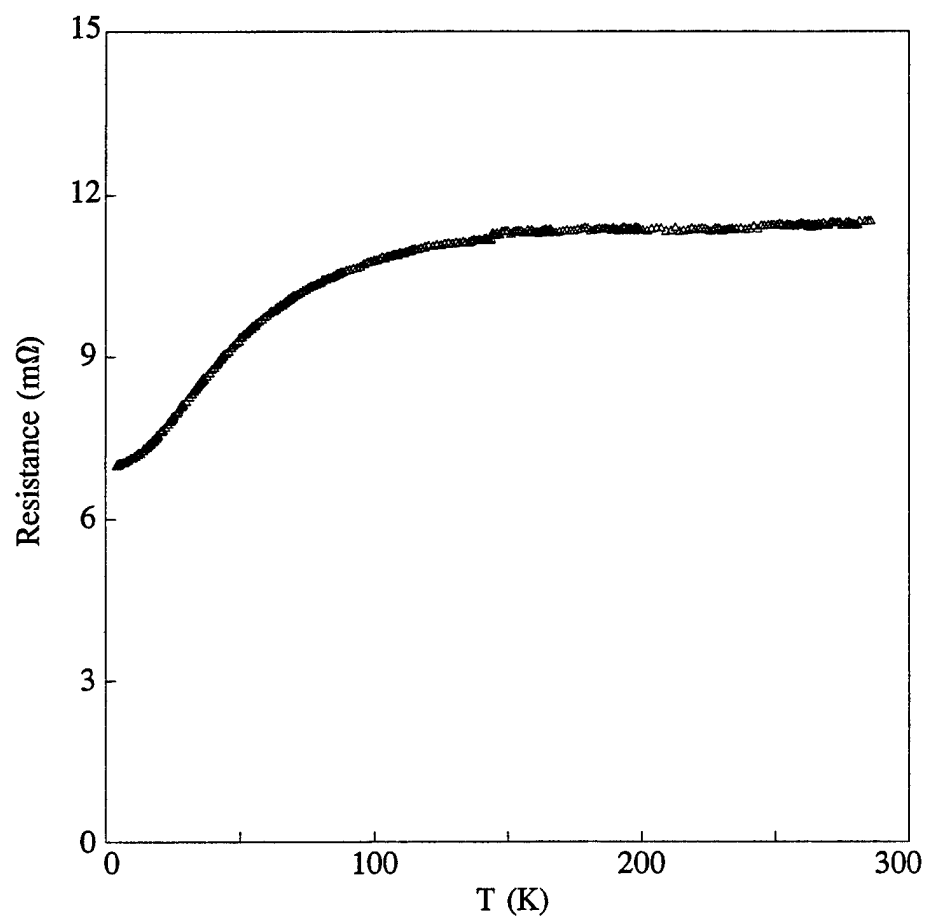


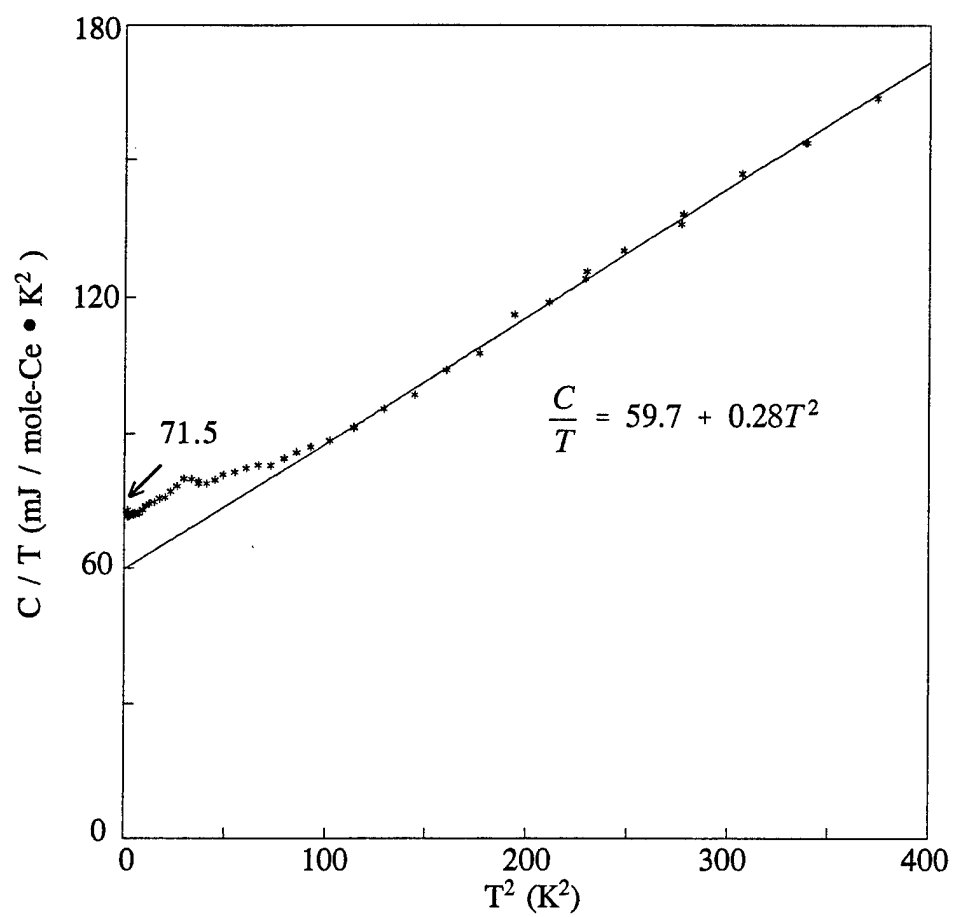












# Technical Report Distribution List

Dr. John C. Pazik (1)\*  
Physical S&T Division - ONR 331  
Office of Naval Research

800 N. Quincy St.  
Arlington, VA 22217-5660

Defense Technical Information  
Ctr (2)  
Building 5, Cameron Station  
Alexandria, VA 22314

Chemistry Division, Code 385  
NAWCWD - China Lake  
China Lake, CA 93555-6001

Dr. James S. Murday  
(1)  
Chemistry Division, NRL 6100  
Naval Research Laboratory  
Washington, DC 20375-5660

Dr. Peter Seligman (1)  
NCCOSC - NRAD  
San Diego, CA 92152-5000

Dr. Bernard E. Douda (1)  
Crane Division  
NAWC

Dr. John Fischer (1)

Crane, Indiana 47522-5000

\* Number of copies required